

pubs.acs.org/acscatalysis Research Article

# Cobalt-Group 13 Complexes Catalyze CO<sub>2</sub> Hydrogenation via a Co(-I)/Co(I) Redox Cycle

Matthew V. Vollmer, Ingyun Ye, John C. Linehan, Brendan J. Graziano, Andrew Preston, Eric S. Wiedner, and Connie C. Lu\*



Cite This: ACS Catal. 2020, 10, 2459–2470



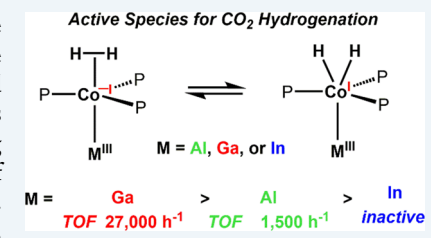
**ACCESS** 

III Metrics & More

Article Recommendations

s Supporting Information

**ABSTRACT:** The Co(-I) dihydrogen complexes,  $[(\eta^2-H_2)\text{CoML}]^-$ , where ML is the group 13 metalloligand, N(o-(NCH $_2$ P $^i$ Pr $_2$ )C $_6$ H $_4$ ) $_3$ M, and M is Al, Ga, or In, were previously reported (*J. Am. Chem. Soc.* **2017**, 139, 6570–6573). In this work, the related Co(-I) end-on dinitrogen adducts,  $[(N_2)\text{CoML}]^-$ , were isolated and investigated as precatalysts for CO $_2$  hydrogenation. The Co–Ga catalyst was highly active, achieving 19,200 formate turnovers with an initial turnover frequency of 27,000 h $^{-1}$  under 34 atm of 1:1 CO $_2$ /H $_2$  and using Verkade's proazaphosphatrane as a base at ambient temperature. The Co–Al catalyst was moderately active, while the Co–In complex was inactive. Hence, tuning the group 13 ion greatly influences the catalytic activity at the Co site. To elucidate



the role of the group 13 support, experimental and theoretical mechanistic studies of the Co–Ga and Co–Al catalysts were conducted. The Co(–I)  $H_2$  species are potent hydride donors with estimated thermodynamic hydricities ( $\Delta G^{\circ}_{H-}$ ) of 32.0(1) and 37.4(1) kcal/mol in CH<sub>3</sub>CN for M = Al and Ga, respectively. By acting as masked Co(I) dihydrides, the Co(–I)  $H_2$  species operate via an unusual Co(–I)/Co(I) redox cycle. After hydride transfer to CO<sub>2</sub>, the resulting intermediate is the Co(I) hydride complex, HCoML, which was independently synthesized and structurally characterized for M = Al and Ga. The Gibbs free energy for  $H_2$  binding,  $\Delta G^{\circ}_{bind}$  (1 atm), to generate ( $\eta^2$ -H<sub>2</sub>)HCoML was slightly more favorable for HCoGaL (–4.2(1) kcal/mol) than for HCoAlL (–2.7(1) kcal/mol). In the subsequent step, the deprotonation reaction to regenerate the initial catalyst was much more favorable for ( $\eta^2$ -H<sub>2</sub>)HCoGaL ( $pK_a$  of 31.4, CH<sub>3</sub>CN) than for ( $\eta^2$ -H<sub>2</sub>)HCoAlL ( $pK_a$  of 34.3). The straightforward substitution of Al with Ga perturbs the energy profile of the catalytic reaction ( $|\Delta\Delta G^{\circ}_{H-}| = 5.4$  kcal/mol,  $|\Delta\Delta G^{\circ}_{bind}| = 1.5$  kcal/mol, and  $|\Delta\Delta G^{\circ}_{K_a}| = 4.0$  kcal/mol) and thus provides a thermodynamic rationale for the higher catalytic efficiency of Co–Ga over Co–Al.

KEYWORDS: cobalt, gallium, carbon dioxide, hydrogenation, Z ligand, hydricity

#### INTRODUCTION

The hydrogenation of  $\mathrm{CO}_2$  to formic acid is particularly attractive as it utilizes an abundant  $\mathrm{C}_1$  feedstock ( $\mathrm{CO}_2$ ) to produce a value-added commodity chemical and an alternative transportation fuel via release of  $\mathrm{H_2}$ . For large-scale  $\mathrm{HCO}_2\mathrm{H}$  production, sustainable catalytic processes are desired, which ideally use earth-abundant metal ions and operate at ambient conditions without a base or other additives. Within the past decade, much effort has focused on developing first-row transition metal catalysts for  $\mathrm{CO}_2$  hydrogenation, particularly iron and cobalt. Nearly all these catalysts generate formate. However, the performance of base metal catalysts continues to lag behind those of the state-of-the-art precious metals, and vast improvements are still needed. Provided the state-of-the-art precious metals, and vast improvements are still needed.

The catalytic competency of cobalt in  $CO_2$  hydrogenation was established early on through screening studies, where HCo-(diphos)<sub>2</sub> or Co salts mixed with diphosphine ligands were found to have limited activity. In 2012, the Co tetraphosphine complex,  $[Co(H)_2(P(CH_2CH_2PPh_2)_3]BF_4$  (Figure 1a), was reported to catalyze the hydrogenation of  $CO_2$  or NaHCO<sub>3</sub> to formate, where a large turnover number, ~4000, was achieved for NaHCO<sub>3</sub> with 60 bar H<sub>2</sub> and heating to

120 °C.<sup>20</sup> The HCo(dmpe)<sub>2</sub> catalyst (Figure 1b) was notable for its turnover frequency (TOF) of 3400 h<sup>-1</sup> at ambient temperature and pressure (1 atm  $CO_2/H_2$ ) in THF but required the use of the strong base, Verkade's proazaphosphatrane. 22,23 Increasing the CO<sub>2</sub>/H<sub>2</sub> pressure to 20 atm resulted in a remarkable TOF of 74,000 h<sup>-1</sup>. Replacing dmpe with a tetraphosphine ligand with pendant amines generated a Co complex (Figure 1c) that is catalytically less active (TOF of 150-180 h<sup>-1</sup>) but operates with the significantly weaker guanidine base and ambient conditions.<sup>25</sup> Impressive activity was reported for the phosphine-based pincer complex [Co- $(^{iPr}PNP)(CO)_2]^+$  (Figure 1d) with ~30,000 turnovers and TOF of 5700 h<sup>-1</sup> using an even weaker base, DBU.<sup>24</sup> Drawbacks of this system include the necessity of the Lewis acidic additive LiOTf for high activity, harsher conditions (68 atm  $CO_2/H_2$ , 45 °C), and observation of a free ligand resulting from catalyst

Received: August 19, 2019 Revised: January 4, 2020 Published: January 13, 2020



Figure 1. (a-f) Co-based catalysts for  $CO_2$  hydrogenation. (g) Cogroup 13 complexes in this study.

heterogenization. Perhaps, among the Co-phosphine-type complexes, the most intriguing catalyst is the mixture of  $Co(acac)_3$ , triphos, and  $Tf_2NH$  (Figure 1e) because it is a rare base metal catalyst that forms methanol from  $CO_2$  and  $H_2$ . The mechanism favoring methanol is not fully clear. Based on rates, the authors have suggested that neither formic acid nor CO is an intermediate en route to methanol. Last, several Co catalysts have been shown to operate in aqueous solution. The  $[CoCp^*(DHBP)(OH_2)]^+$  catalyst (Figure 1f) is unique because it lacks phosphine donors and operates in aqueous bicarbonate solution to produce formate at a rate of  $39 \, h^{-1}$  ( $40 \, atm \, CO_2/H_2$ ,  $80 \, ^{\circ}C$ ). In aqueous bicarbonate solution, the  $HCo(dmpe)_2$  complex is protonated to afford a different active species,  $[(H)_2Co(dmpe)_2]^+$ , which displays a TOF of  $560 \, h^{-1}$  ( $34 \, atm \, CO_2/H_2$ ,  $100 \, ^{\circ}C$ ) for production of formate.

With these limited number of precedents, Co catalysts appear promising for further development. In organic solvents, the Cophosphine catalysts are postulated to operate via a Co(I)/ Co(III) redox cycle involving Co(I)H and Co(III) dihydride species.  $^{20,22,25}$  While the Co(I)/Co(III) redox cycle is commonly invoked in molecular Co-based catalysis,<sup>33</sup> other plausible redox cycles that feature lower valent Co, such as Co(0) and Co(-I), are emerging. 34–38 Our group has been leveraging Lewis acidic group 13 metalloligands to stabilize lowvalent, first-row metal centers and to enhance base metal reactivity. Broadly,  $\sigma$ -accepting, Z-type ligands are gaining traction as a useful tool to control transition metal (TM) reactivity in catalysis, where the TM  $\rightarrow$  Z direct bonding interaction can dynamically tune the TM electron density. 44-While main group Lewis acids are known to interact with metal hydrides, typically, the hydride bridges the TM and main group centers, rendering the hydride less hydridic.<sup>48</sup> We recently reported a NiGaL catalyst for CO2 hydrogenation (L is [N(o-(NCH<sub>2</sub>P<sup>i</sup>Pr<sub>2</sub>)C<sub>6</sub>H<sub>4</sub>)<sub>3</sub>]<sup>3-</sup>), where a terminal reactive hydride, H–Ni  $\rightarrow$  Ga, was stabilized due to the strong inverse transinfluence of the Ga Lewis acid.<sup>49,50</sup> In a related work, Takaya and Iwasawa investigated group 13 metalloligands in Pd-catalyzed CO<sub>2</sub> hydrosilylation.<sup>51</sup> The Al metalloligand showed a significant boost in catalytic activity over that of Ga and In, but the origin of the effect was unclear.

The current work details the isoelectronic  $d^{10}$  Co analogues and their efficacy in CO<sub>2</sub> hydrogenation. Specifically, the Co(-I) H<sub>2</sub> adducts,  $[(\eta^2 - H_2) \text{CoML}]^-$  (Figure 1g), which were

shown to be isolable, are ideal for investigating the influence of the group 13 metal ion on catalytic activity, in particular because such studies are rare. Our mechanistic and thermodynamic studies provide evidence that the Co(-I)  $H_2$  species acts as a masked Co(I) dihydride, which is sufficiently hydridic to transfer to  $CO_2$ . Moreover, the group 13 center plays an important role in tuning the  $pK_a$  and thermodynamic hydricity. Also, these Co-group 13 catalysts engage in a rare Co(-I)/Co(I) redox cycle that facilitates  $CO_2$  hydrogenation with comparable activity to the state-of-the-art base-metal catalysts.

## ■ RESULTS AND DISCUSSION

Synthesis and Characterization of the [(N<sub>2</sub>)CoML]<sup>-</sup> **Precatalysts.** The  $H_2$  adducts of the Co(-I)/group 13 bimetallic complexes,  $[(\eta^2-H_2)CoML]^-$ , were previously reported for M = Al, Ga, and In, which will be referred to as  $[\hat{1}-H_2]^-$ ,  $[2-H_2]^-$ , and  $[3-H_2]^-$ , respectively. Preliminary experiments showed that both [1-H<sub>2</sub>] and [2-H<sub>2</sub>] generated formate and a clean metal product (vide infra) when exposed to a 1:1 mixture of  $CO_2/H_2$  (1.8 atm). We surmised that both [1- $H_2$  and  $[2-H_2]$  must be sufficiently hydridic to fully transfer a hydride to CO<sub>2</sub>. For further studies, we switched to using the bis(triphenylphosphine) iminium (PPN) salts of the  $Co(-I) N_2$ complexes,  $[(N_2)CoML]^-([1-N_2]^- to [3-N_2]^-)$ , as precatalysts because of their synthetic ease and high crystallization yields. The PPN salts of  $[1-N_2]^-$  to  $[3-N_2]^-$  were all prepared similarly in a one-pot reaction: the group 13 metalloligand, ML, and CoCl<sub>2</sub> were stirred in THF, followed by separate additions of 3.1 equiv of Na/Hg and [PPN][tetrakis(3,5-bis(trifluoromethyl)phenyl)borate] 56,57 (see Experimental Section for details and Figures S1 and S2). Single crystals of [PPN][2-N2] and [PPN][3-N<sub>2</sub>] were grown from THF/Et<sub>2</sub>O, and the solidstate structures obtained from X-ray diffraction studies are shown in Figure 2 (Tables S1 and S2). The structure of

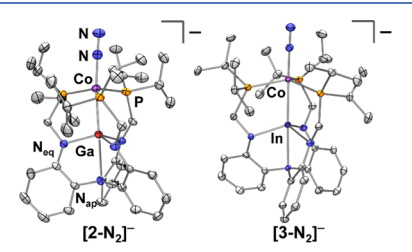


**Figure 2.** Solid-state structures of the precatalysts  $[PPN][2-N_2]$  and  $[PPN][3-N_2]$ . Thermal ellipsoids are shown at 50% probability. The PPN cation, H atoms, and noncoordinating solvents are omitted for clarity.

[Li(crypt-222)][1-N<sub>2</sub>]<sup>-</sup> was reported previously. <sup>41</sup> Cyclic voltammetry (CV) of this series showed a reversible Co(0/-1) redox potential that shifts anodically as M is varied down group 13:  $E_{1/2}$  values are -1.76, -1.65, and -1.56 V versus  $FeCp_2^{+/0}$  for  $[1-N_2]^-$ ,  $[2-N_2]^-$ , and  $[3-N_2]^-$ , respectively (Figures S3–S5). Solutions of  $[(N_2)CoML]^-$  all rapidly converted to the corresponding  $H_2$  adducts upon exposure to  $H_2$  gas (1.8 atm). Hence, they were judged to be suitable precatalysts for further hydrogenation studies. The Co(0/-1) redox potentials for  $[1-H_2]^-$  and  $[2-H_2]^-$  were also measured and were similar to their  $N_2$  counterparts with  $E_{1/2} = -1.79$  and -1.66 V, respectively (Figures S8 and S9 and Table S3).

**Catalyst Screening.** The [PPN][(N<sub>2</sub>)CoML] precatalysts were tested for CO<sub>2</sub> hydrogenation under identical conditions

ACS Catalysis pubs.acs.org/acscatalysis Research Article

that had been described for the isoelectronic NiGaL catalyst. <sup>49</sup> In a standard catalytic run, a high-pressure PEEK cell was loaded with catalyst (0.25 mM, 0.031 mol %), Verkade's proazaphosphatrane (2,8,9-triisopropyl-2,5,8,9-tetraazaphosphabicyclo[3.3.3]-undecane; abbreviated as Vkd)<sup>58</sup> as the stoichiometric base, THF- $d_8$ , and a constant pressure (34 atm) of 1:1 CO<sub>2</sub>/H<sub>2</sub>. The plot of the formate turnovers versus time, as monitored by <sup>1</sup>H nuclear magnetic resonance (NMR) spectroscopy at 293 K, is shown in Figure 3 for the three precatalysts.

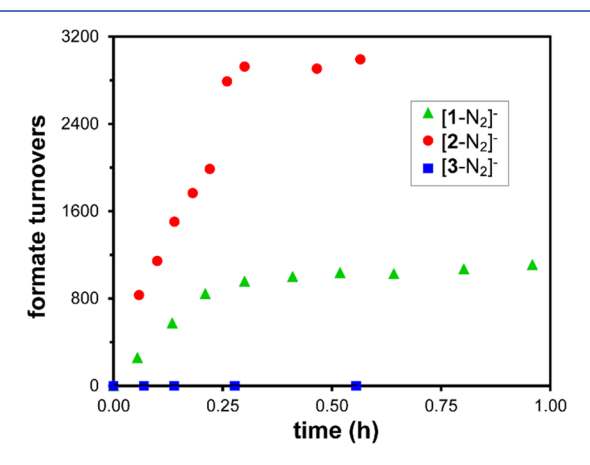


**Figure 3.** Plot of formate turnovers versus time in  $CO_2$  hydrogenation reactions using  $[1-N_2]^-$  to  $[3-N_2]^-$ . Catalytic conditions: 0.25 mM precatalyst, 800 mM Vkd, 34 atm of 1:1  $CO_2/H_2$ , 293 K. Average value of duplicate trials for  $[1-N_2]^-$  and  $[2-N_2]^-$ . Single trial for  $[3-N_2]^-$ .

While  $[3-N_2]^-$  is completely inactive, both  $[1-N_2]^-$  and  $[2-N_2]^-$  generated formate with an initial turnover frequency (TOF) of 1500 and 11,000 h<sup>-1</sup>, respectively (Table 1, entries 1–3). Moreover,  $[2-N_2]^-$  achieved a high formate yield of 97%.

Next, we sought to optimize the Co–Ga catalyst system. By decreasing the concentration of  $[2\text{-N}_2]^-$  to 0.063 and 0.030 mM (~0.008 and 0.004 mol %, respectively), the formate turnovers increased by 4- and 6-fold to 12,000 and 19,000, respectively (entries 4 and 5). While entry 5 gave the highest turnovers and TOF (27,000 h<sup>-1</sup>) in this study, the formate yield plateaued at

72%. The incomplete reaction is possibly due to partial catalyst decomposition, which can be problematic at low catalyst concentrations. The initial TOFs for entries 3 and 4 are consistent with a reaction that is first order with respect to the catalyst. The TOF for entry 5 is  $\sim$ 25% lower than expected for first-order catalyst dependence, but this discrepancy may be explained by the partial catalyst decomposition.

We further probed the robustness and/or efficiency of the Co–Ga catalyst system by varying other catalytic parameters such as pressure, the  $\rm CO_2/H_2$  ratio, and the choice of the stoichiometric base. While lowering the  $\rm CO_2/H_2$  (1:1) pressure to 17 atm did not impact the overall formate yield (98%, entry 6), the TOF nearly halved (c.f. entry 3). Upon further lowering of the  $\rm CO_2/H_2$  pressure to 1 or 1.8 atm, the formate yield decreased substantially (<30%, entries 7 and 8). From these results, we infer that catalyst stability is interdependent on both the catalyst concentration and  $\rm CO_2/H_2$  pressure.

The ratio of the CO<sub>2</sub>/H<sub>2</sub> gases is also critical to the catalytic performance of [2-N<sub>2</sub>]-. A 1:3 ratio of CO<sub>2</sub>/H<sub>2</sub>, under otherwise standard conditions, negatively affected both the formate yield and TOF (entry 9). On the other hand, inverting the CO<sub>2</sub>/H<sub>2</sub> ratio to 3:1 did not affect the high yield of formate and even increased the TOF slightly to  $13,000 \, h^{-1}$  (entry 10). By evaluating the TOFs at different CO<sub>2</sub> partial pressures (entries 3, 6, and 10), we approximate that the reaction is first order with respect to  $P_{CO_2}$ . These entries also suggest a zeroth order rate dependence on PH, with the caveat that H2-rich gas streams have a deleterious effect (entry 9). While we do not yet understand why catalytic performance suffers under 1:3 CO<sub>2</sub>/  $H_2$  gas, we do note that the  $[(\eta^2-H_2)CoML]^-$  species are stable under H<sub>2</sub> for prolonged periods. We suspect that the catalyst decomposes to [2-CO]-, where the CO is likely produced by decarbonylation of formic acid.<sup>23</sup> In support, heating a postcatalytic sample at 55 °C overnight forms a new Co species with a single broad  $^{31}P$  NMR peak at  $\sim$ 78 ppm. The assignment of the carbonyl product was confirmed by an independent synthesis of [PPN] [2-CO] from the reaction of ethyl formate and [2-N<sub>2</sub>] (see Experimental Section and Supporting Information).

Table 1. Catalytic CO<sub>2</sub> Hydrogenation to Formate under Various Conditions<sup>a</sup>

entry	precatalyst	loading (mM)	base	P <sub>total</sub> (atm)	$CO_2/H_2$	initial TOF $(h^{-1})^b$	formate turnovers <sup>c</sup>	% yield <sup>d</sup>
1	$[1-N_2]^-$	0.25	Vkd	34	1:1	1500	1900 <sup>e</sup>	59
2	$[3-N_2]^-$	0.25	Vkd	34	1:1	0	0	0
3	$[2-N_2]^-$	0.25	Vkd	34	1:1	1100	3100	97
4	$[2-N_2]^-$	0.063	Vkd	34	1:1	23,000	12,000	98
5	$[2-N_2]^-$	0.030	Vkd	34	1:1	27,000	19,000	72
6	$[2-N_2]^-$	0.25	Vkd	17	1:1	5000	3200	98
7	$[2-N_2]^-$	0.25	Vkd	1.8	1:1	530	950 <sup>e</sup>	30
8	$[2-N_2]^-$	1.2	Vkd	1	1:1	64	160	24
9	$[2-N_2]^-$	0.25	Vkd	34	1:3	2500	1200	37
10	$[2-N_2]^-$	0.25	Vkd	34	3:1	13,000	3200	98
11	$[2-N_2]^-$	2.0	tBuTMG	34	1:1	2300	480 <sup>f</sup>	>99
12	$[2-N_2]^-$	2.0	DBU	34	1:1	1400	360 <sup>g</sup>	90
13	$[2-N_2]^-$	20	NEt <sub>3</sub>	34	1:1	not calculated	<2.5 <sup>h</sup>	<6

"Conditions: precatalyst (0.030 to 20 mM), 800 mM base, 350  $\mu$ L of THF- $d_8$ , 293 K. For further details, see Experimental Section. Values are averages of duplicate catalytic trials, except for entries 3 (triplicate) and 13 (single). t = 1.5 h, unless otherwise specified. See Table S4 for results of individual trials. Initial TOF is the slope of formate turnovers versus time at initial time, typically the first 15–20 min where the plot is linear. Formate turnovers based on H NMR integration using an internal capillary standard. Assuming that the base is the limiting reagent. t = 6 h; initial TOF decreases sharply after t = 1 h. Turnover exceeds base equivalents, implying that both formate and formic acid are formed. No internal standard was used to prevent precipitation of  $[H(DBU)][CO_2H]$ . Formate was integrated against the PPN cation.

The strength of the base is an important factor in catalytic  $CO_2$  hydrogenation to formate. For both  $HCo(dmpe)_2$  and NiGaL, strong bases such as Vkd, whose conjugate acid has a  $pK_a$  of 33.6 in  $CH_3CN$ , <sup>60</sup> were shown to enhance catalytic activity. In the present Co-Ga system, Vkd can be replaced by substantially weaker bases while retaining high formate yields. For example, tert-butyl tetramethyl guanidine (abbreviated as  $^tBuTMG$ ;  $pK_a$  of 26.5) <sup>61</sup> and 1,8-diazabicyclo[5.4.0]undec-7-ene (abbreviated as DBU;  $pK_a$  of 24.34) <sup>62</sup> achieved  $\geq$ 360 turnovers, although increasing the catalyst concentration to 2.0 mM was necessary (entries 11 and 12, Figures S11 and S12). <sup>59</sup> On the other hand, using  $NEt_3$  ( $pK_a$  of 18.8) as the stoichiometric base effectively shuts down catalysis (entry 13).

Stoichiometric Reactivity and Characterization of Intermediates. To shed some light on plausible intermediates, stoichiometric reactions were conducted using the [PPN]- $[(N_2)CoML]$  complexes as a starting point (Figure 4). For [1-

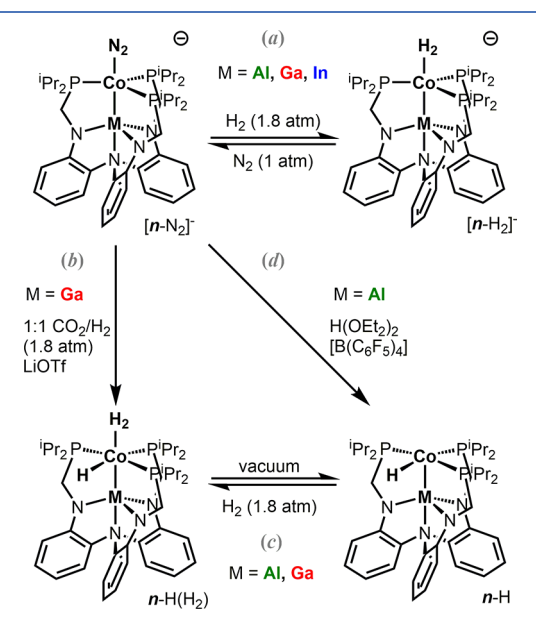


**Figure 4.** Starting from [PPN][( $N_2$ )CoML], the syntheses of [PPN][( $\eta^2$ -H<sub>2</sub>)CoML], [PPN][n-H<sub>2</sub>]; ( $\eta^2$ -H<sub>2</sub>)HCoML, n-H(H<sub>2</sub>); and HCoML, n-H. Note that n is 1 (M = Al), 2 (M = Ga), or 3 (M = In).

 $N_2$ ]<sup>-</sup>,  $[2-N_2]$ <sup>-</sup>, and  $[3-N_2]$ <sup>-</sup>, the  $N_2$  ligand was displaced by  $H_2$  under 1.8 atm  $H_2$  (Figure 4, eqs a, and eqs S16 and S17). This ligand exchange was readily reversed by replacing the headspace with  $N_2$ . Exposure of  $[PPN][2-N_2]$  to both  $CO_2$  and  $H_2$  (1:1, 1.8 atm) resulted in the appearance of formate (8.6 ppm) and a very broad  $^1H$  NMR resonance at -8.1 ppm that integrated to 3H per ligand (Figure S18). We propose that the latter product is ( $\eta^2$ - $H_2$ )HCoGaL, 2-H( $H_2$ ), which is the  $H_2$  adduct of the Co(I) hydride species HCoGaL (2-H). Both of these Co(I) hydride species, 2-H and 2-H( $H_2$ ), were synthesized independently to validate their assignments and to support their intermediacy. The Co-Al system  $[1-N_2]$  was also studied and showed a similar reactivity profile (Figure S19). The Co-In system  $[3-N_2]$  was not further investigated because of its poor catalytic activity.

Complex 2-H was isolated after workup from the addition of 1.8 atm  $CO_2/H_2$  (1:1) to a thawing THF solution of [PPN][2- $N_2$ ] and LiOTf (Figure 4, eq b). The addition of LiOTf was helpful to precipitate both Li( $O_2CH$ ) and [PPN]OTf. The

solution color changed from an initial bright yellow to dark green and finally to a pale yellow color upon warming. These color changes are consistent with the chemical transformation of  $[2\text{-N}_2]^-$  to 2-H and then to 2-H(H<sub>2</sub>) (vide infra). Upon exposure to vacuum, the filtrate reverted to a dark green color, from which 2-H was isolated as a dichroic purple-green microcrystalline powder in 92% yield (Figure 4, eq c). Single crystals of 2-H were grown from  $\text{Et}_2\text{O}/\text{pentane}$  solutions as dark indigo plates, and the resulting X-ray diffraction crystal structure is displayed in Figure 5 (Tables S1 and S2). The geometry of the

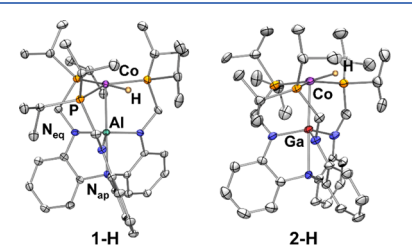


**Figure 5.** Solid-state structures of 1-H and 2-H. Thermal ellipsoids are shown at 50% probability. The ligand H atoms and noncoordinating solvents are omitted for clarity. Two independent molecules in each unit cell.

Co center in 2-H is distorted square pyramidal, where the hydride atom resides slightly out-of-plane with respect to the three phosphorus nuclei. This distortion likely results from steric congestion of the phosphines' isopropyl substituents and further twists the ligand arms such that the two trans-disposed phosphines become chemically inequivalent (vide infra). The Co–Ga distance of 2.4057(9) Å is shorter than the sum of the metals' covalent radii (2.48 Å),<sup>64</sup> which indicates a significant Co  $\rightarrow$  Ga dative interaction.

The NMR characterization for 2-H was performed at a low temperature to resolve its fluxional behavior in solution. At -18 °C, the hydride signal appears as an apparent triplet of doublets ( $^2J_{\rm H-P}=82$  and 48 Hz), which collapses into a singlet at -15.68 ppm upon  $^{31}{\rm P}$  decoupling that integrated to 1H (Figures S20 and S28). The  $^{31}{\rm P}\{^1{\rm H}\}$  NMR spectrum consists of broad features at room temperature that sharpens into three distinct peaks at -25 °C: two doublets at 67.4 and 48.8 ppm ( $^2J_{\rm P-P}=142$  Hz) and a sharp singlet at 64.2 ppm (Figure S21). The two doublets correspond to the trans-disposed phosphine nuclei, which are magnetically inequivalent. A similar phenomenon was previously described for the isostructural Rh analogue HRhGaL.

The Co–Al hydride HCoAlL (1-H) was isolated from the protonation of [PPN][1-N<sub>2</sub>] using H(Et<sub>2</sub>O)<sub>2</sub>[B(C<sub>6</sub>F<sub>5</sub>)<sub>4</sub>] as a blue-colored microcrystalline powder in 72% yield (Figure 4d). The hydride resonance for 1-H appears as a triplet of doublets ( $^2J_{\rm H-P}$  = 102 and 55 Hz) at –15.18 ppm (Figures S22 and S23). The solid-state structure of 1-H is isostructural to that of 2-H (Figure 5), with a distorted square pyramidal Co center. The Co–Al distance of 2.458(2) Å is slightly shorter than the sum of the metals' covalent radii (2.47 Å).

As an aside, the deep colors of the HCoML species arise from two intense absorptions in the visible region,  $\lambda_{\rm max}$  in nm ( $\varepsilon$  in L mol<sup>-1</sup> cm<sup>-1</sup>): 480 (3600)/600 (2400) for 1-H and 510 (3900)/630 (2300) for 2-H (Figure S29). To understand the nature of these excitations, time-dependent density functional theory (TD-DFT) calculations were performed on the HCoML species at the M06-L level of theory (see Computational Methods). The predicted excitation energies agree well with the experimental

Figure 6. DFT-calculated mechanism for the hydrogenation of CO<sub>2</sub> to formate by the Co-Ga catalyst, [2-H<sub>2</sub>]<sup>-</sup>. Two pathways (paths A and B) are shown. For additional pathways, see Figures S37 and S38.

values (Tables S5–S9). Hence, these bands are assigned as electronic transitions from Co  $\rm d_{zz}/L(\pi)$  and Co  $\rm d_{yz}/d_{xy}$  to the lowest unoccupied molecular orbital (LUMO), which is composed of atomic orbitals on Co (4p<sub>z</sub>), the group 13 center (p<sub>z</sub> and s), and P (p<sub>z</sub>). A similar LUMO was previously reported for the NiML triad<sup>66</sup> and identified as the frontier acceptor orbital in small-molecule binding, as well as single-electron reduction. Hence, in analogy to the NiML triad, we propose that H<sub>2</sub> binding to HCoML involves a donor—acceptor interaction between  $\sigma(H_2)$  and the LUMO. This donor—acceptor interaction also rationalizes the stark color changes of 1-H/2-H upon exposure to H<sub>2</sub> since these excitations would be quenched.

The complexes  $1-H(H_2)$  and  $2-H(H_2)$  are the formal  $H_2$ adducts of 1-H and 2-H, respectively. These species were spectroscopically characterized in situ because of the lability of the  $H_2$  ligand. Any of the synthetic routes to 1-H/2-H shown in Figure 4 were also effective for generating 1-H( $H_2$ )/2-H( $H_2$ ), simply by introducing or maintaining H<sub>2</sub> in the headspace of the reaction. Both 1-H(H<sub>2</sub>) and 2-H(H<sub>2</sub>) are characterized by a broad <sup>1</sup>H NMR resonance at -7.80 and -8.08 ppm, respectively, in THF- $d_8$  at room temperature that integrates to 3H (Figures S24–S27). Upon cooling to -82 °C, this resonance for 2-H(H<sub>2</sub>) decoalesces into two very broad resonances at approximately -3 and -18 ppm, with approximate integrations of 2H and 1H, respectively. These observations support the assignment of a Co dihydrogen-hydride species, where the H<sub>2</sub> and hydride atoms are in rapid exchange. <sup>63</sup> For  $1-H(H_2)$ , even with cooling to -90 °C, the single  $H_2/H$  peak did not decoalesce, suggesting an even lower kinetic barrier for H<sub>2</sub>/H exchange compared to  $2-H(H_2)$ . The dihydrogen-hydride assignment for 1-H(H<sub>2</sub>) and 2-H(H<sub>2</sub>), rather than a metal trihydride, is also consistent with the measured spin-lattice relaxation times  $(T_{1(min)})^{68}$  of 23.8 and 24.9 ms (500 MHz, -40 and -25 °C), respectively (Figure S30). These values are within the norm of both  $Co(H_2)$  complexes and  $CoH(H_2)$  complexes, where the spin-lattice relaxation is enhanced by large dipolar

couplings between H atoms and the I=7/2 <sup>59</sup>Co nucleus. <sup>69</sup> By removing these dipolar contributions to the  $T_{1(\min)}$  value as well as the contribution of the Co–H (Figure S31) and assuming the rapid rotation of the H<sub>2</sub> ligand, we can approximate  $d_{\rm H-H}$  to be 0.85(1) and 0.86(1) Å for 1-H(H<sub>2</sub>) and 2-H(H<sub>2</sub>), respectively (Tables S10 and S11). <sup>70</sup> The H–H bond lengths are contracted compared to  $[1\text{-H}_2]^-$  and  $[2\text{-H}_2]^-$ , c.f. 0.97(1) and 0.98(1) Å, respectively. The extent of H<sub>2</sub> activation is consistent with their different formal oxidation states, Co(I) versus Co(–I). Last, both 1-H(H<sub>2</sub>) and 2-H(H<sub>2</sub>) incorporate deuterium readily upon exposure to either HD or a 1:1 H<sub>2</sub>/D<sub>2</sub> gas mixture.

**Catalytic Mechanism.** The catalytic mechanism of the Co–Ga system was investigated using a combined experimental and theoretical approach. The catalyst resting state was scrutinized using in situ NMR spectroscopy at a sufficiently high catalyst loading (20 mM). When the base was Vkd, the resting state was identified as  $[2\text{-H}_2]^-$  based on its characteristic <sup>31</sup>P NMR chemical shift and <sup>1</sup>H NMR resonance at -7.7 ppm (Figure S32). On the other hand, swapping Vkd with a weaker base changes the catalytic resting state to its conjugate acid,  $2\text{-H}(H_2)$  (Figure S33). These observations demonstrate that the identity of the rate-limiting step is dependent on base strength. In the strong base limit, hydride transfer from  $[2\text{-H}_2]^-$  to  $CO_2$  is rate-determining. While in the weak base limit, deprotonation of  $2\text{-H}(H_2)$  becomes slower than hydride transfer.

DFT calculations were performed on  $[2\text{-H}_2]^-$ , 2-H, and 2-H(H<sub>2</sub>) to obtain optimized geometries (M06-L, <sup>71</sup> see Computational Methods; Figures S35—S38). When feasible, the X-ray coordinates were used as the initial geometry, and solvation effects were accounted for with the SMD model. <sup>72</sup> The DFT energies were performed at 298.15 K, which is slightly higher than the experimental temperature of 293 K. Overall,  $\Delta G^{\circ}$  for the overall reaction  $H_2(g) + CO_2(g) + Vkd(sol) \rightleftharpoons [HVkd]$ - $[HCO_2](sol)$  is predicted to be +6.1 kcal/mol. The  $\Delta G^{\circ}$  value varies significantly across different functionals: M06-2X functional yields a less endergonic change of +2.3 kcal/mol, and wB97XD predicts an exergonic change of -2.0 kcal/mol. Of

ACS Catalysis pubs.acs.org/acscatalysis Research Article

note, the M06-2X and wB97XD functionals were designed for organic systems, not for transition metals.<sup>73</sup> Moreover, M06-L, which is suited to both organic systems and transition metals, gave the best agreement to experimental structures and binding energies for the related Ni-group 13 complexes.<sup>66</sup>

One energetically favorable reaction pathway, path A, is shown in Figure 6, with the reaction coordinate diagram in Figure 7. The complex  $[2-H_2]^-$ , which is formally a Co(-I)  $H_2$ 

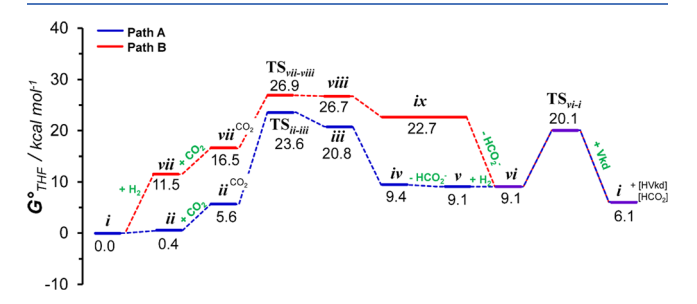


**Figure 7.** DFT-calculated reaction coordinate diagram for paths A and B ( $G^{\circ}$  in kcal/mol). Although CO<sub>2</sub> does not bind directly to the Co–Ga complex in  $ii^{CO2}$  (or  $vii^{CO2}$ ), the proximity of CO<sub>2</sub> to ii/vii perturbs  $G^{\circ}$ . See Table S12 for a detailed list of all Gibbs free energies.

adduct (i in Figure 6, calculated  $d_{\rm H-H}$  = 0.88 Å) and its oxidative addition isomer, the Co(I) dihydride (ii, calculated  $d_{\rm H-H}$  = 1.81 Å), are nearly isoenergetic, where the latter is 0.4 kcal/mol uphill in energy relative to the former. The H<sub>2</sub> activation step (i to ii) represents an unusual Co(-I)/Co(I) redox reaction. The critical step of hydride transfer from [ $\mathbf{2}$ -H<sub>2</sub>] $^-$  (i to iii, via ii) to CO<sub>2</sub> has a calculated free-energy barrier ( $\Delta G^{\ddagger}$ ) of 23.6 kcal/mol (Figure 8). The formate ligand in the resulting [ $\mathbf{2}$ -H(O<sub>2</sub>CH)] $^-$ 

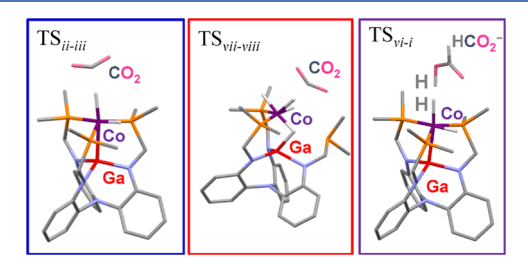


**Figure 8.** DFT-calculated transition-state structure for hydride transfer to  $CO_2$  in path A (blue box) and path B (red box) and  $H_2$  deprotonation via a formate shuttle (purple box). Note that all geometries were optimized with the full ligand. The  $P^iPr_2$  groups are truncated in these images for clarity.

intermediate is initially H-bound (iii) prior to rearranging to the more stable O-bound isomer (iv),  $\Delta G^{\circ} = -11.4$  kcal/mol. Likely, this isomerization process occurs by releasing formate to form 2-H (v), which can rebind formate to form iii. In the forward direction, release of formate from  $[2\text{-H}(O_2\text{CH})]^-$  to generate 2-H is slightly favored with  $\Delta G^{\circ} = -0.3$  kcal/mol. This is notable because formate release is typically rate-limiting for many catalysts. Here, formate release is likely assisted by the anionic charge of the formate adduct. The subsequent binding of H<sub>2</sub> to 2-H forming 2-H(H<sub>2</sub>) (vi, calculated  $d_{H-H} = 0.84$  Å) is thermoneutral. As an aside, we considered an alternative reaction where 2-H binds  $CO_2$  prior to  $CO_2$  insertion into the Co-H bond. We were able to discount this possibility because the  $CO_2$  binding energy to 2-H is predicted to be highly endergonic: 20.8 kcal/mol. Also, the reaction of 2-H and 1 atm

 $CO_2$  is very sluggish, with a  $t_{1/2}$  of 50 min (Figure S34, c.f. [2-H<sub>2</sub>]<sup>-</sup> reacts instantaneously with  $CO_2$ ).

The deprotonation of 2-H(H<sub>2</sub>) is the last key step because it regenerates [2-H<sub>2</sub>]<sup>-</sup>. The deprotonation step was scrutinized for both Vkd and formate. In a prior DFT study of NiGaL, we uncovered that formate can act as a proton shuttle by transferring a proton from the Ni(H<sub>2</sub>) species to the exogenous base. The significantly lower barrier associated with the direct deprotonation by formate compared to Vkd was attributed by unfavorable steric clashes associated in the transition state for Vkd. Likewise, the deprotonation of 2-H(H<sub>2</sub>) by formate has a moderate  $\Delta G^{\ddagger}$  of 11 kcal/mol (Figure 8). The transition-state structure,  $TS_{vi-i}$  in Figure 8, shows that formate deprotonates the H<sub>2</sub> ligand to generate both formic acid and ii, which can then relax to i. Overall, this calculated pathway is consistent with hydride transfer being rate-limiting and lends support to the intermediacy of both 2-H and 2-H(H<sub>2</sub>).

An alternative mechanism, path B, was also calculated to be competitive (Figures 6 and 7). Beginning with [2-H<sub>2</sub>], the first step is dissociation of a phosphine donor and association of a second H2 molecule to yield a Co(I) dihydride dihydrogen species,  $Co(\eta^2-H_2)(H)_2$  (vii). Although the formation of this intermediate is endergonic ( $\Delta G^{\circ} = 11.5 \text{ kcal/mol}$ ), the lower barrier associated with hydride transfer to  $CO_2$  ( $\Delta G^{\ddagger} = 15.4$ kcal/mol) results in a competitive overall barrier of 26.9 kcal/ mol (i to viii, via vii). The hydride transfer step is further interesting because it is formally a Co(I)/Co(III) redox reaction (vii to viii). Inspection of the transition-state structure reveals a Co(III) trihydride (Figure 8). After formate release and reductive coupling of two Co hydrides, 2-H(H<sub>2</sub>) is regenerated. The subsequent deprotonation is the same as that in path A. Path B also affirms rate-limiting hydride transfer and supports the intermediacy of 2-H(H<sub>2</sub>). Overall, it features two twoelectron redox steps, Co(-I)/Co(I) and Co(I)/Co(III).

Binding Equilibria,  $pK_a$ , and Thermodynamic Hydricity. Considering the proposed mechanism, we sought to experimentally measure the  $H_2$  binding free energy to 2-H, which is the reverse of eq 1, and the  $pK_a$  of 2-H(H<sub>2</sub>), which can be extracted from the acid—base equilibria between 2-H(H<sub>2</sub>) and an exogeneous base, as shown in eq 2. With these values in hand, one can further evaluate the thermodynamic hydricity of  $[2\text{-H}_2]^-$  (eq 5)<sup>74,75</sup> using the thermodynamic relationships shown below, including the known  $pK_a$  of the base (eq 3) and the  $H_2$  heterolysis constant (in CH<sub>3</sub>CN, eq 4)

$$2-H(H_2) \rightleftharpoons 2-H + H_2, \Delta G^{\circ}_1 = -\Delta G^{\circ}_{bind}$$
 (1)

 $[2-H_2]^- + BaseH^+$ 

 $\Rightarrow$  2-H(H<sub>2</sub>) + Base,  $\Delta G^{\circ}$ ,

$$= -RT \ln(K_{\rm eq}) \tag{2}$$

Base + H<sup>+</sup> 
$$\rightleftharpoons$$
 BaseH<sup>+</sup>,  $\Delta G^{\circ}_{3} = -1.364(pK_{a})$  (3)

$$H_2 \rightleftharpoons H^+ + H^-, \Delta G^{\circ}_4 = +76 \text{ kcal/mol}$$
 (4)

net: 
$$[\mathbf{2}\text{-H}_2]^- \rightleftharpoons \mathbf{2}\text{-H} + \text{H}^-, \Delta G^{\circ}_{\text{H}^-} = \sum_{i=1}^4 \Delta G^{\circ}_i$$
 (5)

The equilibrium binding of  $H_2$  to 2-H to form 2-H( $H_2$ ) was studied in toluene with 10%  $H_2$ /Ar from 40 to 95 °C by following the 510 nm absorbance of 2-H using UV-vis spectroscopy (Figures S39 and S40). The van't Hoff analysis

of triplicate studies yielded  $\Delta H^\circ_{\rm bind}$  of -14.4(1) kcal/mol,  $\Delta S^\circ_{\rm bind}$  of -34.6(3) cal/mol·K, and  $\Delta G^\circ_{\rm bind}$  of -4.2(1) kcal/mol, where the standard state is defined as 1 atm  $H_2$ , 298 K, and 1 M for all other species in toluene (Figure S41 and Table S14). We also repeated this analysis for the reaction 1-H +  $H_2 \rightleftharpoons 1$ -H( $H_2$ ), with minor adjustments on the same protocol: 25%  $H_2$ /Ar, 25 to 85 °C, and monitoring of the 480 nm absorbance of 1-H (Figure S42). The van't Hoff analysis of triplicate UV–vis studies gave  $\Delta H^\circ_{\rm bind}$  of -10.5(1) kcal/mol,  $\Delta S^\circ_{\rm bind}$  of -26.3(1) cal/mol·K, and  $\Delta G^\circ_{\rm bind}$  of -2.7(1) kcal/mol (Figure S43 and Table S15). Hence,  $H_2$  binding is more exergonic for 2-H versus 1-H, which is in accordance with our measured  $H_2$  binding trend in the NiML series.

The p $K_2$  of 2-H(H<sub>2</sub>) was determined by measuring the acid base equilibrium constants between 2-H( $H_2$ ) and an exogenous base (1.5 to 2 equiv), as monitored by <sup>1</sup>H NMR spectroscopy. Due to the labile nature of the H2 ligand, these studies were performed under 1 atm H<sub>2</sub> in THF-d<sub>8</sub>, rather than CD<sub>3</sub>CN, which can displace H<sub>2</sub> from the Co center (Table S16). Using the organosuperbase N-[1,3-diisopropyl-4,5-dimethyl-imidazol-2-ylidene]tertbutylamine containing an N-heterocyclic carbene core (p $K_a$  of 30.21 in CH<sub>3</sub>CN<sup>76</sup> and p $K_\alpha$  of 22.64 in THF<sup>77</sup>), an equilibrium constant ( $K_{\rm eq}'$ , where  $K_{\rm eq}$  in eq 2 =  $1/K_{\rm eq}'$ ) of 0.072(6) was determined based on three independent measurements, leading to a p $K_a$  value of 23.8(1) for 2-H(H<sub>2</sub>) in THF (estimated p $K_a$  of 31.4 in CH<sub>3</sub>CN). Assuming that  $K_{eq}$  values are comparable in THF and CH<sub>3</sub>CN solvents, we estimate the thermodynamic hydricity  $\Delta G_{H}^{\circ}$  (eq 5) of [2-H<sub>2</sub>] to be 37.4(1) kcal/mol in CH<sub>3</sub>CN. Hence, hydride transfer from [2- $H_2$ ] to  $CO_2$  ( $\Delta G^{\circ}_H$  of formate = 44 kcal/mol)<sup>78</sup> is exergonic. Alternatively, we report the corresponding thermodynamic hydricity of  $[2-H_2]^-$  in THF versus that of  $H_2$ , or  $\Delta G^{\circ}_{H}^-$  ([2- $H_2$ ]  $-\Delta G_H^{\circ}$  ( $H_2$ ). This can be obtained by summing the  $\Delta G^{\circ}$ 's for eqs 1-3to yield -28.2(1) kcal/mol in THF.

Using a similar protocol, the acid—base equilibrium between 1-H(H<sub>2</sub>) and Vkd yielded  $K_{\rm eq}{}'=0.23(1)$ , which gave an estimated p $K_{\rm a}$  value of 34.3(1) for 1-H(H<sub>2</sub>) in CH<sub>3</sub>CN. Under similar assumptions, the  $\Delta G_{\rm H}^{\circ}$  of [1-H<sub>2</sub>] was estimated to be 32.0(1) kcal/mol in CH<sub>3</sub>CN. Alternatively, we also report the corresponding values in THF: the p $K_{\rm a}$  value for 1-H(H<sub>2</sub>) in THF is 26.4(1), and  $\Delta G_{\rm H}^{\circ}$  ([1-H<sub>2</sub>] versus that of H<sub>2</sub> is –33.3(1) kcal/mol. The hydricity value of [2-H<sub>2</sub>] is quite close to that of HCo(dmpe)<sub>2</sub> ( $\Delta G_{\rm H}^{\circ}$  = 36 kcal/mol in CH<sub>3</sub>CN), while [1-H<sub>2</sub>] is an even more potent hydride donor. The complex [1-H<sub>2</sub>] ranks among the most hydridic first-row and many precious transition metal hydrides.

In comparing 1-H(H<sub>2</sub>) and 2-H(H<sub>2</sub>), the acidity of the bound H<sub>2</sub> ligand differs by nearly 3 pK<sub>a</sub> units. The Ga supporting ion leads to an enhanced lowering of the pK<sub>a</sub>(H<sub>2</sub>) compared to Al. We explain this trend by the greater strength of the Co  $\rightarrow$  Ga interaction, which, in turn, leads to a more electron-deficient Co center that is associated with increased activation of the H<sub>2</sub> ligand via better  $\sigma$ -donation from H<sub>2</sub> to the LUMO of HCoML. On the other hand, the Al support makes the [( $\eta^2$ -H<sub>2</sub>)CoML]<sup>-</sup> complex a stronger hydride donor compared to its Ga counterpart, with a difference in the hydride-transfer driving force of 5 kcal/mol. Overall, these results affirm the opposing favorability of H<sub>2</sub> deprotonation versus hydride transfer.  $^{80,81}$ 

# CONCLUSIONS

The catalytic hydrogenation of  $CO_2$  is demonstrated for Cogroup 13 bimetallic compounds, where a low-valent Co center is bonded directly to the Al or Ga metalloligand, but not to In.

Starting with the Co(-I)  $H_2$  species, oxidative addition of  $H_2$  to obtain the Co(I) dihydride isomer is supported by its ability to transfer a hydride to  $CO_2$  in the absence of an exogenous base, the DFT-calculated reaction energy profile, and the facile scrambling of  $H_2$  and  $D_2$  scrambling. Despite similar extents of  $H_2$  activation in  $\begin{bmatrix} \mathbf{1} \cdot \mathbf{H}_2 \end{bmatrix}^- (0.97 \text{ Å})$  and  $\begin{bmatrix} \mathbf{2} \cdot \mathbf{H}_2 \end{bmatrix}^- (0.98 \text{ Å})$ , the thermodynamic hydricity increases by 5 kcal/mol when Al is switched to Ga. Since hydride transfer to  $CO_2$  is exergonic for both Co-Al and Co-Ga (<44 kcal/mol), the latter is a more efficient hydride donor.

We also investigated the Co(I)H and  $Co(I)H(H_2)$  intermediates and the  $H_2$  binding equilibrium that connects these species.  $\Delta G^{\circ}_{bind}$  at 1 atm  $H_2$  is slightly more exergonic for HCoGaL than for HCoAlL. The  $pK_a$  of  $H(H_2)CoGaL$  is also significantly lower by nearly 3  $pK_a$  units compared to that of  $H(H_2)CoAlL$ , making the former easier to deprotonate and regenerate the active Co(-I)  $H_2$  species. Hence, all the thermodynamic considerations point to Co-Ga being a more efficient catalyst than Co-Al.

The collective experimental evidence supports the Co(-I)/Co(I) redox cycle. Intriguingly, DFT calculations predict another energetically competitive pathway whereby a phosphine donor first dechelates so that a second  $H_2$  equivalent binds to the Co center. In this pathway, the canonical Co(I)/Co(III) redox cycle is also involved, giving an overall four-electron redox cycle.

In optimizing the Co–Ga catalyst, the rate law was approximated to be first order with respect to  $CO_2$  pressure and zeroth order with respect to  $H_2$  pressure. While moderate bases such as 'BuTMG (p $K_a$  of 26.5) and DBU (p $K_a$  of 24.3) are catalytically viable with TOFs of 2300 and 1350 h<sup>-1</sup>, respectively, the significantly stronger Vkd base (p $K_a$  of 33.6) greatly enhances the initial rate up to 27,000 h<sup>-1</sup>. The main drawback of the Co–Ga catalyst is the need for Vkd as a stoichiometric base to achieve  $10^4$  turnovers. Other concerns are signs of catalyst decomposition at exceedingly low catalyst loadings, at low  $CO_2/H_2$  pressures, or when the  $CO_2/H_2$  ratio is 1:3. Future work will aim to simultaneously increase catalyst efficiency and robustness.

# **■ EXPERIMENTAL SECTION**

Synthesis of  $[N(PPh_3)_2][(N_2)CoAl(N(o-(NCH_2P^iPr_2) C_6H_4)_3$ ] ([PPN][1-N<sub>2</sub>]). In an Ar-atmosphere glovebox, a 100 mL Schlenk flask was charged with a stir bar, AlL (408.1 mg, 580  $\mu$ mol), anhydrous CoCl<sub>2</sub> (75.2 mg, 580  $\mu$ mol), and 20 mL of THF. This mixture was stirred for 1-2 h until it was homogeneous, at which point freshly prepared ~1% Na/Hg (41.3 mg Na, 1.80 mmol) was added. The flask was evacuated (opened to static vacuum, ×3) and refilled with ultrahigh-purity  $N_2$  (1 atm). The mixture was stirred overnight and then filtered. The yellow-red filtrate was reduced in vacuo to 6 mL, and then solid [PPN][BArF<sub>24</sub>] (1.00 g, 713  $\mu$ mol) was added with a stir bar. The solution was stirred until solids began to precipitate, and then 15 mL Et<sub>2</sub>O was added. The microcrystalline bright yellow solid was washed with Et<sub>2</sub>O (2  $\times$  10 mL) and dried overnight in vacuo to yield bright yellow crystalline solids (460 mg, 60% yield). Single crystals of [PPN][1-N<sub>2</sub>] were grown from THF/Et<sub>2</sub>O or DME/Et<sub>2</sub>O solutions.

<sup>1</sup>H{<sup>31</sup>P} NMR (THF- $d_8$ , 500 MHz):  $\delta$  7.59–7.45 (overlapping m, 30H, PPN), 7.06 (d, J = 7.5 Hz, 3H, aryl), 6.60 (t, J = 7.6 Hz, 3H, aryl), 6.15 (d, J = 7.9 Hz, 3H, aryl), 5.97 (t, J = 7.4 Hz, 3H, aryl), 2.72 (br, 6H, CH<sub>2</sub>), 2.37 (br, 3H, CH(CH<sub>3</sub>)<sub>2</sub>), 2.01 (br, 3H, C'H(CH<sub>3</sub>)<sub>2</sub>), 1.31 (br, 18H CH(CH<sub>3</sub>)<sub>2</sub>), 0.88 (br, 18H, C'H(CH<sub>3</sub>)<sub>2</sub>). <sup>31</sup>P{<sup>1</sup>H} NMR (THF- $d_8$ , 202 MHz):  $\delta$  56.1

(3P), 21.0 (2P, PPN). IR (KBr pellet):  $\nu(N_2)$  1994 cm<sup>-1</sup>. The spectroscopic properties of this species are identical to those previously reported for  $[K(\text{crypt-222})][1-N_2]$ .

Synthesis of  $[N(PPh_3)_2][(N_2)CoGa(N(o-(NCH_2P^iPr_2)-C_6H_4)_3)]$  ([PPN][2-N<sub>2</sub>]). A similar procedure to that described for [PPN][1-N<sub>2</sub>] was used with the following changes: GaL (471.7 mg, 630  $\mu$ mol), CoCl<sub>2</sub> (81.9 mg, 630  $\mu$ mol), and ~1% NaHg (44.9 mg Na, 1.95 mmol). A bright yellow crystalline solid was obtained (500 mg, 58% yield). Single crystals of [PPN][2-N<sub>2</sub>] were grown by layering Et<sub>2</sub>O onto a DME solution and storing at -30 °C.

<sup>1</sup>H(<sup>31</sup>P) NMR (THF- $d_8$ , 500 MHz):  $\delta$  7.59–7.45 (s, 30H, PPN), 7.02 (d, J = 7.4 Hz, 3H, aryl), 6.56 (t, J = 7.6 Hz, 3H, aryl), 6.13 (d, J = 7.9 Hz, 3H, aryl), 5.94 (t, J = 7.4 Hz, 3H, aryl), 2.79 (br, 3H, CHH'<sub>2</sub>), 2.58 (br, 3H, CHH'<sub>2</sub>), 2.35 (br, 3H, CH(CH<sub>3</sub>)<sub>2</sub>), 2.03 (br, 3H, C'H(CH<sub>3</sub>)<sub>2</sub>), 1.29 (br, 18H, CH(CH<sub>3</sub>)<sub>2</sub>), 0.88 (br, 18H, C'H(CH<sub>3</sub>)<sub>2</sub>).  $^{31}$ P(<sup>1</sup>H) NMR (THF- $d_8$ , 202 MHz):  $\delta$  65.9 (3P), 21.0 (2P, PPN). IR (KBr pellet):  $\nu$ (N<sub>2</sub>) 1999 cm<sup>-1</sup>. Anal. calcd for [PPN][2-N<sub>2</sub>]·DME, [C<sub>36</sub>H<sub>30</sub>NP<sub>2</sub>][C<sub>39</sub>H<sub>60</sub>N<sub>6</sub>P<sub>3</sub>GaCo]·C<sub>4</sub>H<sub>10</sub>O<sub>2</sub> (%): C, 64.85; H, 6.89; N, 6.70. Found: C, 64.75; H, 7.10; N, 5.88. The reproducibly low N content may be related to N<sub>2</sub> loss.

Synthesis of  $[N(PPh_3)_2][(N_2)CoIn(N(o-(NCH_2P^iPr_2)-C_6H_4)_3)]$  ([PPN][3-N<sub>2</sub>]). A similar procedure to that described for [PPN][1-N<sub>2</sub>] was used with the following changes: InL (400.5 mg, 510  $\mu$ mol), CoCl<sub>2</sub> (65.6 mg, 510  $\mu$ mol), and ~1% NaHg (36 mg Na, 1.57 mmol). A yellow crystalline solid was obtained (360 mg, 50% yield).

<sup>1</sup>H{<sup>31</sup>P} NMR (500 MHz, THF- $d_8$ ): δ 7.59–7.45 (m, 30H, PPN), 7.10 (d, J = 7.6 Hz, 3H, aryl), 6.55 (t, J = 7.6 Hz, 3H, aryl), 6.12 (d, J = 8.0 Hz, 3H, aryl), 5.89 (t, J = 7.3 Hz, 3H, aryl), 2.80 (br, 6H, CH<sub>2</sub>), 2.24 (s, 6H, CH(CH<sub>3</sub>)<sub>2</sub>), 1.12 (br, 36H, CH(CH<sub>3</sub>)<sub>2</sub>). <sup>31</sup>P{<sup>1</sup>H} NMR (162 MHz, THF- $d_8$ ): δ 73.7 (3P), 21.0 (2P, PPN). IR (KBr pellet):  $\nu$ (N<sub>2</sub>) 2021 cm<sup>-1</sup>. Anal. calcd for [PPN][2-N<sub>2</sub>], [C<sub>36</sub>H<sub>30</sub>NP<sub>2</sub>][C<sub>39</sub>H<sub>60</sub>N<sub>6</sub>P<sub>3</sub>InCo] (%): C, 63.52; H, 6.40; N, 6.91. Found: C, 63.42; H, 6.66; N, 5.03. The reproducibly low N content may be related to N<sub>2</sub> loss.

**Synthesis of HCoAl(N(o-(NCH<sub>2</sub>P<sup>i</sup>Pr<sub>2</sub>)C<sub>6</sub>H<sub>4</sub>)<sub>3</sub>)] (1-H).** In an N<sub>2</sub>-atmosphere glovebox, a THF solution of  $[H(OEt_2)_2][B-(C_6F_5)_4]^{\$2}$  (77.8 mg, 0.094 mmol, in 2 mL) was added to a THF suspension of  $[PPN][1-N_2]$  (125 mg, 0.094 mmol, in 10 mL) that had been cooled to -30 °C. The reaction, which turned a deep blue color, was stirred for 30 min at room temperature and then dried in vacuo. The residue was extracted with hexane (2 × 15 mL) and filtered. The filtrate was dried in vacuo to yield 51 mg (70% yield) of a deep blue microcrystalline solid, which was stored at -30 °C. NMR data were collected under Ar.  $^1$ H NMR data acquired under N<sub>2</sub> were more complex, indicating N<sub>2</sub> binding.

<sup>1</sup>H NMR (toluene- $d_8$ , 500 MHz, Ar): δ 7.47 (d, J = 7.6 Hz, 3H, aryl), 7.11 (t, J = 7.5 Hz, 3H, aryl), 6.49 (t, J = 7.5 Hz, 3H, aryl), 6.45 (d, J = 7.9 Hz, 3H, aryl), 3.33 (br, 2H, CH<sub>2</sub>), 3.09 (br, 4H, CH<sub>2</sub>), 2.17–2.10 (br, 6H, CH(CH<sub>3</sub>)<sub>2</sub>), 1.00 (br, 36H, CH(CH<sub>3</sub>)<sub>2</sub>), -15.18 (td,  $^2J_{\rm H-P}$  = 102 and 55 Hz, CoH).  $^{31}$ P{ $^{1}$ H} NMR (THF- $d_8$ , 202 MHz, -25 °C): δ 62.7 (d, J = 137 Hz, 1P), 59.5 (s, 1P), 44.9 (d, J = 137 Hz, 1P). Anal. calcd for 1-H·0.5(Et<sub>2</sub>O), C<sub>39</sub>H<sub>61</sub>N<sub>4</sub>P<sub>3</sub>AlCo·0.5(C<sub>4</sub>H<sub>10</sub>O) (%): C, 61.41; H, 8.30; N, 6.99. Found: C, 61.70; H, 8.05; N, 6.75.

Synthesis of  $HCoGa(N(o-(NCH_2P^iPr_2)C_6H_4)_3)]$  (2-H). In an Ar-atmosphere glovebox,  $[PPN][2-N_2]$  (148 mg, 0.11 mmol) and LiOTf (28 mg, 0.18 mmol) were stirred in THF (20 mL) until a homogeneous yellow solution was obtained. This solution was transferred to a Schlenk flask and subjected to

a freeze-pump-thaw cycle. During the thawing, the flask was filled with  $1:1~{\rm H_2/CO_2}$  (1 atm). While it was still cold, the bright yellow solution turned dark green and, upon warming, turned a dull yellow color with white precipitate. After stirring for 1 h at room temperature, the reaction solution was dried in vacuo. The resulting residue was extracted with  ${\rm Et_2O}$  (20 mL) and filtered. The dark green filtrate was then dried in vacuo. The solids were triturated with hexane to obtain a dichroic purple-green microcrystalline powder (80.0 mg, 90% yield).

<sup>1</sup>H{<sup>31</sup>P} NMR (toluene- $d_8$ , 400 MHz): δ 7.50 (d, J = 7.6 Hz, 3H, aryl), 7.09 (t, J = 7.7 Hz, 3H, aryl), 6.50 (t, J = 7.5 Hz, 3H, aryl), 6.46 (d, J = 7.9 Hz, 3H, aryl), 3.24 (br, 2H,  $CH_2$ ), 3.08 (s, 4H,  $CH_2$ ), 2.40–2.13 (br, 6H,  $CH(CH_3)_2$ ), 1.2–0.71 (br, 36H,  $CH(CH_3)_2$ ), -15.68 (s, 1H, CoH). At -18 °C, <sup>1</sup>H NMR: δ -15.45 (td, J = 82 and 47.5 Hz, CoH). <sup>31</sup>P{<sup>1</sup>H} NMR (162 MHz, toluene- $d_8$ ): δ 64.9 (s). At -25 °C, <sup>31</sup>P{<sup>1</sup>H} NMR: δ 67.4 (d, J = 142 Hz, 1P), 64.2 (s, 1P), 48.8 (d, J = 142 Hz, 1P). Anal. calcd for 2-H,  $C_{39}H_{61}N_4P_3GaCo$  (%): C, 58.01; H, 7.61; N, 6.94. Found: C, 56.24; H, 7.87; N, 6.30. The elemental analyses repeatedly failed, presumably because of the extreme air sensitivity of 2-H.

High-Pressure Catalytic Reactions. Caution: H<sub>2</sub> is a highly flammable gas. Pressurized vessels must be handled with care using proper personal protective equipment. CO<sub>2</sub> hydrogenation reactions were performed in PEEK high-pressure NMR spectroscopy tubes that were designed and built at Pacific Northwest National Laboratory. 83 In a typical catalytic experiment of 0.25 mM catalyst and 800 mM base, a 0.20 mL aliquot of a [PPN][2-N<sub>2</sub>] stock solution (2.6 mg, 1.89  $\mu$ mol, 2 mL of THF-d<sub>8</sub>) was added to a THF-d<sub>8</sub> solution of Vkd (180 mg in 0.55 mL) to obtain a total reaction volume of 0.75 mL. For duplicate catalytic trials, two PEEK NMR cells were each loaded with 350  $\mu$ L of the reaction solution and a capillary of CoCl<sub>2</sub> in D<sub>2</sub>O to serve as an internal standard. The PEEK cell was sealed and connected to a purged high-pressure line equipped with a vacuum pump and an ISCO syringe pump. The headspace was degassed by opening the PEEK cell to static vacuum ( $3 \times 10 \text{ s}$ ). Gas was delivered to the cell from an ISCO syringe pump running constantly at the desired pressure (typically 34 atm, continuous gas feed). The contents of the PEEK cells were mixed using a vortex mixer for ~3 min until the pressure stabilized. After stabilization, the cell was inserted periodically into the NMR spectrometer to acquire data. <sup>1</sup>H NMR spectra were collected every 3–5 min using the following parameters: eight scans each, delay time of 1 s, acquisition time of 5 s, pulse width of 4  $\mu$ s (20° pulse), and gain of 2 (totaling 48 s per spectrum). The concentration of formate was determined by <sup>1</sup>H NMR integration relative to the residual HDO resonance (5.6 ppm) of the CoCl<sub>2</sub>/D<sub>2</sub>O standard. The <sup>31</sup>P spectra were collected at the same time interval, with four scans per spectrum, a delay time of 5 s, and an acquisition time of 5 s (totaling 21 s per spectrum). The contents of the PEEK cell were mixed using a vortex mixer when NMR data were not being collected to promote optimal gas-liquid mixing during the catalytic trial.

**Computational Methods.** Density functional theory (DFT) calculations were performed with Gaussian 09 software. <sup>84</sup> Geometries were optimized in the gas phase with the M06-L<sup>71</sup> functional and the following basis sets: def2-TZVPP for Co, Ga, and any atoms directly involved in the reaction (e.g., atoms in CO<sub>2</sub>, CO, HCO<sub>2</sub><sup>-</sup>, H<sup>-</sup>, H<sub>2</sub>O, and H<sub>2</sub>); def2-TZVP for N and P; and def2-SVP basis set for any invariant C and H atoms. <sup>85</sup> The M06-L functional and the above basis sets gave the best match to the experimental geometries and binding

energies for the related Ni-group 13 complexes.<sup>66</sup> In addition, the geometry of 2-H was optimized using five different functionals, and M06-L gave the best match to the experimental structure (Table S13). Harmonic vibrational frequencies were computed and confirmed the nature of all intermediates (no imaginary frequencies) and transition-state structures (one imaginary frequency). The gas-phase Gibbs free energies, G, were calculated at T = 298.15 K and 1 atm pressure by using the harmonic approximation for the optimized structures. The solvation effect of tetrahydrofuran (THF) was included by performing single-point energy calculations at the gas-phase geometries using the SMD solvation model.<sup>72</sup> The relative solution-phase Gibbs free energies were calculated by adding solvation energies to the gas-phase relative Gibbs free energies. Gibbs free energies are reported for a standard state of 298.15 K, 1 atm for gases, and 1 M for solutes and include the solvent effect of THF (Table S12).

TD-DFT calculations were performed on the M06-L-optimized structures of 1-H and 2-H with solvent considerations (SMD and THF). The M06 hybrid functional <sup>86</sup> with Grimme's dispersion D3 damping function and 6-31G(d,p) basis sets was used.

#### ASSOCIATED CONTENT

# Supporting Information

The Supporting Information is available free of charge at https://pubs.acs.org/doi/10.1021/acscatal.9b03534.

Additional data for synthesis, catalysis, characterization, and DFT calculations (PDF)

Crystallographic data for  $[PPN][2-N_2]$ ,  $[PPN][3-N_2]$ , 1-H, and 2-H (CIF)

Combined XYZ coordinates of DFT-optimized geometries (XYZ)

## AUTHOR INFORMATION

### **Corresponding Author**

Connie C. Lu — Department of Chemistry, University of Minnesota—Twin Cities, Minneapolis, Minnesota 55455, United States; orcid.org/0000-0002-5162-9250; Email: clu@umn.edu

#### Authors

Matthew V. Vollmer – Department of Chemistry, University of Minnesota–Twin Cities, Minneapolis, Minnesota 55455, United States

Jingyun Ye — Department of Chemistry and Supercomputing Institute, and Chemical Theory Center, University of Minnesota—Twin Cities, Minneapolis, Minnesota 55455, United States; ⊕ orcid.org/0000-0003-4373-9625

John C. Linehan — Catalysis Science Group, Pacific Northwest National Laboratory, Richland, Washington 99352, United States; © orcid.org/0000-0001-8942-7163

Brendan J. Graziano — Department of Chemistry, University of Minnesota—Twin Cities, Minneapolis, Minnesota 55455, United States; Occid.org/0000-0003-1449-9255

Andrew Preston — Catalysis Science Group, Pacific Northwest National Laboratory, Richland, Washington 99352, United States

Eric S. Wiedner — Catalysis Science Group, Pacific Northwest National Laboratory, Richland, Washington 99352, United States

Complete contact information is available at:

# https://pubs.acs.org/10.1021/acscatal.9b03534

#### **Author Contributions**

M.V.V. and J.Y. contributed equally to this work.

#### Notes

The authors declare no competing financial interest. The CIF files have been deposited to the Cambridge CCDC 1945085 to 1945088.

#### ACKNOWLEDGMENTS

The authors thank Aaron Appel (PNNL) for hosting M.V.V. for the DOE fellowship and Victor Young, Jr. for the crystallographic assistance. At UMN, Laura Gagliardi and Don Truhlar are thanked for helpful discussion. M.V.V. was supported by the DOE Office of Science Graduate Student Research and the UMN Doctoral Dissertation fellowships. C.C.L. and B.J.G. were supported by the NSF (CHE-1665010). J.Y. was supported as part of the Inorganometallic Catalyst Design Center, an Energy Frontier Research Center funded by the U.S. Department of Energy (DOE), Office of Science, Basic Energy Sciences, under award DE-SC0012702. J.C.L., A.P., and E.S.W. were supported by the U.S. Department of Energy, Office of Science, Office of Basic Energy Sciences, Division of Chemical Sciences, Geosciences & Biosciences.

#### REFERENCES

- (1) Sordakis, K.; Tang, C.; Vogt, L. K.; Junge, H.; Dyson, P. J.; Beller, M.; Laurenczy, G. Homogeneous Catalysis for Sustainable Hydrogen Storage in Formic Acid and Alcohols. *Chem. Rev.* **2018**, *118*, 372–433.
- (2) Wang, W.-H.; Himeda, Y.; Muckerman, J. T.; Manbeck, G. F.; Fujita, E.  $CO_2$  Hydrogenation to Formate and Methanol as an Alternative to Photo- and Electrochemical  $CO_2$  Reduction. *Chem. Rev.* **2015**, *115*, 12936–12973.
- (3) Jessop, P. G.; Joó, F.; Tai, C.-C. Recent Advances in the Homogeneous Hydrogenation of Carbon Dioxide. *Coord. Chem. Rev.* **2004**, 248, 2425–2442.
- (4) Francke, R.; Schille, B.; Roemelt, M. Homogeneously Catalyzed Electroreduction of Carbon Dioxide—Methods, Mechanisms, and Catalysts. *Chem. Rev.* **2018**, *118*, 4631–4701.
- (5) Benson, E. E.; Kubiak, C. P.; Sathrum, A. J.; Smieja, J. M. Electrocatalytic and Homogeneous Approaches to Conversion of CO<sub>2</sub> to Liquid Fuels. *Chem. Soc. Rev.* **2009**, *38*, 89–99.
- (6) Mellmann, D.; Sponholz, P.; Junge, H.; Beller, M. Formic Acid as a Hydrogen Storage Material Development of Homogeneous Catalysts for Selective Hydrogen Release. *Chem. Soc. Rev.* **2016**, *45*, 3954—3988.
- (7) Enthaler, S.; von Langermann, J.; Schmidt, T. Carbon Dioxide and Formic Acid-the Couple for Environmental-Friendly Hydrogen Storage? *Energy Environ. Sci.* **2010**, *3*, 1207–1217.
- (8) Artz, J.; Müller, T. E.; Thenert, K.; Kleinekorte, J.; Meys, R.; Sternberg, A.; Bardow, A.; Leitner, W. Sustainable Conversion of Carbon Dioxide: An Integrated Review of Catalysis and Life Cycle Assessment. *Chem. Rev.* **2018**, *118*, 434–504.
- (9) Bullock, R. M., Ed.; Catalysis without Precious Metals; Wiley-VCH: Weinheim, 2010.
- (10) Filonenko, G. A.; van Putten, R.; Hensen, E. J. M.; Pidko, E. A. Catalytic (De)Hydrogenation Promoted by Non-Precious Metals Co, Fe and Mn: Recent Advances in an Emerging Field. *Chem. Soc. Rev.* **2018**, *47*, 1459—1483.
- (11) Bernskoetter, W. H.; Hazari, N. Reversible Hydrogenation of Carbon Dioxide to Formic Acid and Methanol: Lewis Acid Enhancement of Base Metal Catalysts. *Acc. Chem. Res.* **2017**, *50*, 1049–1058.
- (12) Chakraborty, S.; Bhattacharya, P.; Dai, H.; Guan, H. Nickel and Iron Pincer Complexes as Catalysts for the Reduction of Carbonyl Compounds. *Acc. Chem. Res.* **2015**, *48*, 1995–2003.
- (13) Ziebart, C.; Federsel, C.; Anbarasan, P.; Jackstell, R.; Baumann, W.; Spannenberg, A.; Beller, M. Well-Defined Iron Catalyst for

- Improved Hydrogenation of Carbon Dioxide and Bicarbonate. J. Am. Chem. Soc. 2012, 134, 20701–20704.
- (14) Zhang, Y.; MacIntosh, A. D.; Wong, J. L.; Bielinski, E. A.; Williard, P. G.; Mercado, B. Q.; Hazari, N.; Bernskoetter, W. H. Iron Catalyzed CO<sub>2</sub> Hydrogenation to Formate Enhanced by Lewis Acid Co-catalysts. *Chem. Sci.* **2015**, *6*, 4291–4299.
- (15) Zell, T.; Milstein, D. Hydrogenation and Dehydrogenation Iron Pincer Catalysts Capable of Metal-Ligand Cooperation by Aromatization/Dearomatization. *Acc. Chem. Res.* **2015**, *48*, 1979–1994.
- (16) Rivada-Wheelaghan, O.; Dauth, A.; Leitus, G.; Diskin-Posner, Y.; Milstein, D. Synthesis and Reactivity of Iron Complexes with a New Pyrazine-Based Pincer Ligand, and Application in Catalytic Low-Pressure Hydrogenation of Carbon Dioxide. *Inorg. Chem.* **2015**, *54*, 4526–4538.
- (17) Langer, R.; Diskin-Posner, Y.; Leitus, G.; Shimon, L. J. W.; Ben-David, Y.; Milstein, D. Low-Pressure Hydrogenation of Carbon Dioxide Catalyzed by an Iron Pincer Complex Exhibiting Noble Metal Activity. *Angew. Chem., Int. Ed.* **2011**, *50*, 9948–9952.
- (18) Fong, H.; Peters, J. C. Hydricity of an Fe-H Species and Catalytic CO<sub>2</sub> Hydrogenation. *Inorg. Chem.* **2015**, *54*, 5124–5135.
- (19) Zhu, F.; Ling, Z.-G.; Yang, G.; Zhou, S. Iron-Catalyzed Hydrogenation of Bicarbonates and Carbon Dioxide to Formates. *ChemSusChem* **2015**, *8*, 609–612.
- (20) Federsel, C.; Ziebart, C.; Jackstell, R.; Baumann, W.; Beller, M. Catalytic Hydrogenation of Carbon Dioxide and Bicarbonates with a Well-Defined Cobalt Dihydrogen Complex. *Chem. Eur. J.* **2012**, *18*, 72–75
- (21) Badiei, Y. M.; Wang, W.-H.; Hull, J. F.; Szalda, D. J.; Muckerman, J. T.; Himeda, Y.; Fujita, E. Cp\*Co(III) Catalysts with Proton-Responsive Ligands for Carbon Dioxide Hydrogenation in Aqueous Media. *Inorg. Chem.* **2013**, *52*, 12576–12586.
- (22) Jeletic, M. S.; Mock, M. T.; Appel, A. M.; Linehan, J. C. A Cobalt-Based Catalyst for the Hydrogenation of CO<sub>2</sub> under Ambient Conditions. *J. Am. Chem. Soc.* **2013**, *135*, 11533–11536.
- (23) Jeletic, M. S.; Helm, M. L.; Hulley, E. B.; Mock, M. T.; Appel, A. M.; Linehan, J. C. A Cobalt Hydride Catalyst for the Hydrogenation of CO<sub>2</sub>: Pathways for Catalysis and Deactivation. *ACS Catal.* **2014**, *4*, 3755–3762.
- (24) Spentzos, A. Z.; Barnes, C. L.; Bernskoetter, W. H. Effective Pincer Cobalt Precatalysts for Lewis Acid Assisted CO<sub>2</sub> Hydrogenation. *Inorg. Chem.* **2016**, *55*, 8225–8233.
- (25) Burgess, S. A.; Grubel, K.; Appel, A. M.; Wiedner, E. S.; Linehan, J. C. Hydrogenation of  ${\rm CO_2}$  at Room Temperature and Low Pressure with a Cobalt Tetraphosphine Catalyst. *Inorg. Chem.* **2017**, *56*, 8580–8589
- (26) Schneidewind, J.; Adam, R.; Baumann, W.; Jackstell, R.; Beller, M. Low-Temperature Hydrogenation of Carbon Dioxide to Methanol with a Homogeneous Cobalt Catalyst. *Angew. Chem., Int. Ed.* **2017**, *56*, 1890–1893.
- (27) Tanaka, R.; Yamashita, M.; Nozaki, K. Catalytic Hydrogenation of Carbon Dioxide Using Ir(III)-Pincer Complexes. *J. Am. Chem. Soc.* **2009**, *131*, 14168–14169.
- (28) Filonenko, G. A.; Hensen, E. J. M.; Pidko, E. A. Mechanism of CO<sub>2</sub> Hydrogenation to Formates by Homogeneous Ru-PNP Pincer Catalyst: from a Theoretical Description to Performance Optimization. *Catal. Sci. Technol.* **2014**, *4*, 3474–3485.
- (29) Tai, C.-C.; Chang, T.; Roller, B.; Jessop, P. G. High-Pressure Combinatorial Screening of Homogeneous Catalysts: Hydrogenation of Carbon Dioxide. *Inorg. Chem.* **2003**, *42*, 7340–7341.
- (30) Inoue, Y.; Sasaki, Y.; Hashimoto, H. Synthesis of Formates from Alcohols, Carbon Dioxide, and Hydrogen Catalyzed by a Combination of Group VIII Transition Metal Complexes and Tertiary Amines. *J. Chem. Soc., Chem. Commun.* **1975**, 718–719.
- (31) Kar, S.; Goeppert, A.; Kothandaraman, J.; Prakash, G. K. S. Manganese-Catalyzed Sequential Hydrogenation of CO<sub>2</sub> to Methanol via Formamide. *ACS Catal.* **2017**, *7*, 6347–6351.
- (32) Burgess, S. A.; Appel, A. M.; Linehan, J. C.; Wiedner, E. S. Changing the Mechanism for CO<sub>2</sub> Hydrogenation Using Solvent-

- Dependent Thermodynamics. Angew. Chem., Int. Ed. 2017, 56, 15002–15005.
- (33) Tokmic, K.; Markus, C. R.; Zhu, L.; Fout, A. R. Well-Defined Cobalt(I) Dihydrogen Catalyst: Experimental Evidence for a Co(I)/Co(III) Redox Process in Olefin Hydrogenation. *J. Am. Chem. Soc.* **2016**, *138*, 11907–11913.
- (34) Büschelberger, P.; Gärtner, D.; Reyes-Rodriguez, E.; Kreyenschmidt, F.; Koszinowski, K.; Jacobi von Wangelin, A.; Wolf, R. Alkene Metalates as Hydrogenation Catalysts. *Chem. Eur. J.* **2017**, 23, 3139–3151.
- (35) Chirik, P. J. Iron- and Cobalt-Catalyzed Alkene Hydrogenation: Catalysis with Both Redox-Active and Strong Field Ligands. *Acc. Chem. Res.* **2015**, *48*, 1687–1695.
- (36) Gärtner, D.; Welther, A.; Rad, B. R.; Wolf, R.; Jacobi von Wangelin, A. Heteroatom-Free Arene-Cobalt and Arene-Iron Catalysts for Hydrogenations. *Angew. Chem., Int. Ed.* **2014**, *53*, 3722–3726.
- (37) Friedfeld, M. R.; Margulieux, G. W.; Schaefer, B. A.; Chirik, P. J. Bis(phosphine)cobalt Dialkyl Complexes for Directed Catalytic Alkene Hydrogenation. *J. Am. Chem. Soc.* **2014**, *136*, 13178–13181.
- (38) Gianetti, T. L.; Rodríguez-Lugo, R. E.; Harmer, J. R.; Trincado, M.; Vogt, M.; Santiso-Quinones, G.; Grützmacher, H. Zero-Valent Amino-Olefin Cobalt Complexes as Catalysts for Oxygen Atom Transfer Reactions from Nitrous Oxide. *Angew. Chem., Int. Ed.* **2016**, 55, 15323–15328.
- (39) Cammarota, R. C.; Clouston, L. J.; Lu, C. C. Leveraging Molecular Metal-Support Interactions for H<sub>2</sub> and N<sub>2</sub> Activation. *Coord. Chem. Rev.* **2017**, 334, 100–111.
- (40) Cammarota, R. C.; Lu, C. C. Tuning Nickel with Lewis Acidic Group 13 Metalloligands for Catalytic Olefin Hydrogenation. *J. Am. Chem. Soc.* **2015**, *137*, 12486–12489.
- (41) Rudd, P. A.; Planas, N.; Bill, E.; Gagliardi, L.; Lu, C. C. Dinitrogen Activation at Iron and Cobalt Metallalumatranes. *Eur. J. Inorg. Chem.* **2013**, 2013, 3898–3906.
- (42) Rudd, P. A.; Liu, S.; Gagliardi, L.; Young, V. G., Jr.; Lu, C. C. Metal-Alane Adducts with Zero-Valent Nickel, Cobalt, and Iron. *J. Am. Chem. Soc.* **2011**, 133, 20724–20727.
- (43) Vollmer, M. V.; Xie, J.; Cammarota, R. C.; Young, V. G., Jr.; Bill, E.; Gagliardi, L.; Lu, C. C. Formal Nickelate(-I) Complexes Supported by Group 13 Ions. *Angew. Chem., Int. Ed.* **2018**, *57*, 7815–7819.
- (44) Anderson, J. S.; Rittle, J.; Peters, J. C. Catalytic Conversion of Nitrogen to Ammonia by an Iron Model Complex. *Nature* **2013**, *501*, 84–87.
- (45) You, D.; Gabbaï, F. P. Tunable σ-Accepting, Z-Type Ligands for Organometallic Catalysis. *Trends Chem.* **2019**, *1*, 485–496.
- (46) Bouhadir, G.; Bourissou, D. Complexes of Ambiphilic Ligands: Reactivity and Catalytic Applications. *Chem. Soc. Rev.* **2016**, 45, 1065–1079
- (47) Yamashita, M. The Organometallic Chemistry of Boron-Containing Pincer Ligands based on Diazaboroles and Carboranes. *Bull. Chem. Soc. Jpn.* **2016**, *89*, 269–281.
- (48) Maity, A.; Teets, T. S. Main Group Lewis Acid-Mediated Transformations of Transition-Metal Hydride Complexes. *Chem. Rev.* **2016**, *116*, 8873–8911.
- (49) Cammarota, R. C.; Vollmer, M. V.; Xie, J.; Ye, J.; Linehan, J. C.; Burgess, S. A.; Appel, A. M.; Gagliardi, L.; Lu, C. C. A Bimetallic Nickel–Gallium Complex Catalyzes CO<sub>2</sub> Hydrogenation via the Intermediacy of an Anionic *d*<sup>10</sup> Nickel Hydride. *J. Am. Chem. Soc.* **2017**, *139*, 14244–14250.
- (50) Ye, J.; Cammarota, R. C.; Xie, J.; Vollmer, M. V.; Truhlar, D. G.; Cramer, C. J.; Lu, C. C.; Gagliardi, L. Rationalizing the Reactivity of Bimetallic Molecular Catalysts for CO<sub>2</sub> Hydrogenation. *ACS Catal.* **2018**, *8*, 4955–4968.
- (51) Takaya, J.; Iwasawa, N. Synthesis, Structure, and Catalysis of Palladium Complexes Bearing a Group 13 Metalloligand: Remarkable Effect of an Aluminum-Metalloligand in Hydrosilylation of CO<sub>2</sub>. *J. Am. Chem. Soc.* **2017**, *139*, 6074–6077.
- (52) Vollmer, M. V.; Xie, J.; Lu, C. C. Stable Dihydrogen Complexes of Cobalt(-I) Suggest an Inverse trans-Influence of Lewis Acidic Group 13 Metalloligands. *J. Am. Chem. Soc.* **2017**, *139*, 6570–6573.

- (53) Charles, R. M., III; Yokley, T. W.; Schley, N. D.; DeYonker, N. J.; Brewster, T. P. Hydrogen Activation and Hydrogenolysis Facilitated By Late-Transition-Metal—Aluminum Heterobimetallic Complexes. *Inorg. Chem.* **2019**, *58*, 12635—12645.
- (54) Heinekey, D. M.; van Roon, M. Dihydride Complexes of the Cobalt and Iron Group Metals: An Investigation of Structure and Dynamic Behavior. *J. Am. Chem. Soc.* **1996**, *118*, 12134–12140.
- (55) Heinekey, D. M.; Liegeois, A.; van Roon, M. Cationic Dihydrogen Complexes of Rhodium and Cobalt: A Reinvestigation. *J. Am. Chem. Soc.* **1994**, *116*, 8388–8389.
- (56) Fujiki, K.; Kashiwagi, M.; Miyamoto, H.; Sonoda, A.; Ichikawa, J.; Kobayashi, H.; Sonoda, T. Syntheses and Lipophilicities of Tetraarylborate Ions Substituted with Many Trifluoromethyl Groups. *J. Fluorine Chem.* **1992**, *57*, 307–321.
- (57) Yakelis, N. A.; Bergman, R. G. Safe Preparation and Purification of Sodium Tetrakis[(3,5-trifluoromethyl)phenyl]borate (NaBArF<sub>24</sub>): Reliable and Sensitive Analysis of Water in Solutions of Fluorinated Tetraarylborates. *Organometallics* **2005**, 24, 3579–3581.
- (58) Wróblewski, A. E.; Pinkas, J.; Verkade, J. G. Strongly Basic Proazaphosphatranes: P(EtNCH<sub>2</sub>CH<sub>2</sub>)<sub>3</sub>N and P(*iso*-PrNCH<sub>2</sub>CH<sub>2</sub>)<sub>3</sub>N. *Main Group Chem.* **1995**, *1*, 69–79.
- (59) Hansen, P. E.; Lund, T.; Krake, J.; Spanget-Larsen, J.; Hvidt, S. A Reinvestigation of the Ionic Liquid Diisopropylethylammonium Formate by NMR and DFT Methods. *J. Phys. Chem. B* **2016**, *120*, 11279—11286.
- (60) Kisanga, P. B.; Verkade, J. G.; Schwesinger, R. p $K_a$  Measurements of P(RNCH<sub>2</sub>CH<sub>2</sub>)<sub>3</sub>N. J. Org. Chem. **2000**, 65, 5431–5432.
- (61) Zall, C. M.; Linehan, J. C.; Appel, A. M. A Molecular Copper Catalyst for Hydrogenation of CO<sub>2</sub> to Formate. *ACS Catal.* **2015**, *5*, 5301–5305.
- (62) Kaljurand, I.; Kütt, A.; Sooväli, L.; Rodima, T.; Mäemets, V.; Leito, I.; Koppel, I. A. Extension of the Self-Consistent Spectrophotometric Basicity Scale in Acetonitrile to a Full Span of 28 pKa Units: Unification of Different Basicity Scales. *J. Org. Chem.* **2005**, *70*, 1019–1028
- (63) Doherty, M. D.; Grant, B.; White, P. S.; Brookhart, M. Reactions of  $H_2$  and  $R_3$ SiH with Electrophilic Cobalt(III) Alkyl Complexes: Spectroscopic Characterization, Dynamics, and Chemistry of [Cp\*Co-(L)(H)( $\eta^2$ -HSiR<sub>3</sub>)][B-(ArF)<sub>4</sub>]. Organometallics **2007**, 26, 5950–5960.
- (64) Cordero, B.; Gómez, V.; Platero-Prats, A. E.; Revés, M.; Echeverría, J.; Cremades, E.; Barragán, F.; Alvarez, S. Covalent Radii Revisited. *Dalton Trans.* **2008**, 2832–2838.
- (65) Moore, J. T.; Smith, N. E.; Lu, C. C. Structure and Dynamic NMR Behavior of Rhodium Complexes Supported by Lewis Acidic Group 13 Metallatranes. *Dalton Trans.* **2017**, *46*, 5689–5701.
- (66) Cammarota, R. C.; Xie, J.; Burgess, S. A.; Vollmer, M. V.; Vogiatzis, K. D.; Ye, J.; Linehan, J. C.; Appel, A. M.; Hoffmann, C.; Wang, X.; Young, V. G.; Lu, C. C. Thermodynamic and Kinetic Studies of  $\rm H_2$  and  $\rm N_2$  Binding to Bimetallic Nickel-Group 13 Complexes and Neutron Structure of a Ni( $\eta^2$ -H<sub>2</sub>) Adduct. *Chem. Sci.* **2019**, *10*, 7029–7042.
- (67) Vollmer, M. V.; Cammarota, R. C.; Lu, C. C. Reductive Disproportionation of CO<sub>2</sub> Mediated by Bimetallic Nickelate(-I)/Group 13 Complexes. *Eur. J. Inorg. Chem.* **2019**, 2019, 2140–2145.
- (68) Hamilton, D. G.; Crabtree, R. H. An NMR Method for Distinguishing Classical from Nonclassical Structures in Transition Metal Polyhydrides. *J. Am. Chem. Soc.* **1988**, *110*, 4126–4133.
- (69) Desrosiers, P. J.; Cai, L.; Lin, Z.; Richards, R.; Halpern, J. Assessment of the "T1 Criterion" for Distinguishing between Classical and Nonclassical Transition-Metal Hydrides: Hydride Relaxation Rates in Tris(triarylphosphine)osmium Tetrahydrides and Related Polyhydrides. J. Am. Chem. Soc. 1991, 113, 4173–4184.
- (70) Bautista, M. T.; Earl, K. A.; Maltby, P. A.; Morris, R. H.; Schweitzer, C. T.; Sella, A. Estimation of the H-H Distances of  $\eta^2$ -Dihydrogen Ligands in the Complexes Trans-[ $M(\eta^2$ -H<sub>2</sub>)(H)-(PR<sub>2</sub>CH<sub>2</sub>CH<sub>2</sub>PR<sub>2</sub>)<sub>2</sub>]<sup>+</sup> [M = Fe, Ru, R = Ph; M = Os, R = Et] by Solution NMR Methods. *J. Am. Chem. Soc.* **1988**, *110*, 7031–7036.

- (71) Zhao, Y.; Truhlar, D. G. A New Local Density Functional for Main-Group Thermochemistry, Transition Metal Bonding, Thermochemical Kinetics, and Noncovalent Interactions. *J. Chem. Phys.* **2006**, *125*, 194101–194118.
- (72) Marenich, A. V.; Cramer, C. J.; Truhlar, D. G. Universal Solvation Model Based on Solute Electron Density and on a Continuum Model of the Solvent Defined by the Bulk Dielectric Constant and Atomic Surface Tensions. *J. Phys. Chem. B* **2009**, *113*, 6378–6396.
- (73) Chai, J.-D.; Head-Gordon, M. Long-Range Corrected Hybrid Density Functionals with Damped Atom—Atom Dispersion Corrections. *Phys. Chem. Chem. Phys.* **2008**, *10*, 6615—6620.
- (74) Wiedner, E. S.; Chambers, M. B.; Pitman, C. L.; Bullock, R. M.; Miller, A. J. M.; Appel, A. M. Thermodynamic Hydricity of Transition Metal Hydrides. *Chem. Rev.* **2016**, *116*, 8655–8692.
- (75) Berning, D. E.; Noll, B. C.; DuBois, D. L. Relative Hydride, Proton, and Hydrogen Atom Transfer Abilities of [HM-(diphosphine)<sub>2</sub>]PF<sub>6</sub> Complexes (M = Pt, Ni). *J. Am. Chem. Soc.* **1999**, 121, 11432–11447.
- (76) Kunetskiy, R. A.; Polyakova, S. M.; Vavřik, J.; Císařovă, I.; Saame, J.; Nerut, E. R.; Koppel, I.; Koppel, I. A.; Kütt, A.; Leito, I.; Lyapkalo, I. M. A New Class of Organosuperbases, N-Alkyl- and N-Aryl-1,3-dialkyl-4,5-dimethylimidazol-2-ylidene Amines: Synthesis, Structure,  $pK_{\rm BH+}$  Measurements, and Properties. *Chem. Eur. J.* **2012**, *18*, 3621–3630.
- (77) Saame, J.; Rodima, T.; Tshepelevitsh, S.; Kütt, A.; Kaljurand, I.; Haljasorg, T.; Koppel, I. A.; Leito, I. Experimental Basicities of Superbasic Phosphonium Ylides and Phosphazenes. *J. Org. Chem.* **2016**, *81*, 7349–7361.
- (78) DuBois, D. L.; Berning, D. E. Hydricity of Transition-Metal Hydrides and its Role in CO<sub>2</sub> Reduction. *Appl. Organomet. Chem.* **2000**, *14*, 860–862.
- (79) Waldie, K. M.; Ostericher, A. L.; Reineke, M. H.; Sasayama, A. F.; Kubiak, C. P. Hydricity of Transition-Metal Hydrides: Thermodynamic Considerations for CO<sub>2</sub> Reduction. *ACS Catal.* **2018**, *8*, 1313–1324.
- (80) Mondal, B.; Neese, F.; Ye, S. Control in the Rate-Determining Step Provides a Promising Strategy To Develop New Catalysts for CO<sub>2</sub> Hydrogenation: A Local Pair Natural Orbital Coupled Cluster Theory Study. *Inorg. Chem.* **2015**, *54*, 7192–7198.
- (81) Mondal, B.; Neese, F.; Ye, S. Toward Rational Design of 3d Transition Metal Catalysts for CO<sub>2</sub> Hydrogenation Based on Insights into Hydricity-Controlled Rate-Determining Steps. *Inorg. Chem.* **2016**, *55*, 5438–5444.
- (82) Jutzi, P.; Müller, C.; Stammler, A.; Stammler, H.-G. Synthesis, Crystal Structure, and Application of the Oxonium Acid [H- $(OEt_2)_2$ ]<sup>+</sup>[B( $C_6F_5$ )<sub>4</sub>]. Organometallics **2000**, 19, 1442–1444.
- (83) Yonker, C. R.; Linehan, J. C. Investigation of the Hydroformylation of Ethylene in Liquid Carbon Dioxide. *J. Organomet. Chem.* **2002**, *650*, 249–257.
- (84) Frisch, M. J.; Trucks, G. W.; Schlegel, H. B.; Scuseria, G. E.; Robb, M. A.; Cheeseman, J. R.; Scalmani, G.; Barone, V.; Mennucci, B.; Petersson, G. A.; Nakatsuji, H.; Caricato, M.; Li, X.; Hratchian, H. P.; Izmaylov, A. F.; Bloino, J.; Zheng, G.; Sonnenberg, J. L.; Hada, M.; Ehara, M.; Toyota, K.; Fukuda, R.; Hasegawa, J.; Ishida, M.; Nakajima, T.; Honda, Y.; Kitao, O.; Nakai, H.; Vreven, T.; Montgomery, J. A., Jr.; Peralta, J. E.; Ogliaro, F.; Bearpark, M.; Heyd, J. J.; Brothers, E.; Kudin, K. N.; Staroverov, V. N.; Keith, T.; Kobayashi, R.; Normand, J.; Raghavachari, K.; Rendell, A.; Burant, J. C.; Iyengar, S. S.; Tomasi, J.; Cossi, M.; Rega, N.; Millam, J. M.; Klene, M.; Knox, J. E.; Cross, J. B.; Bakken, V.; Adamo, C.; Cammi, R.; Gomperts, R.; Stratmann, R. E.; Yazyev, O.; Austin, A. J.; Pomelli, C.; Ochterski, J. W.; Martin, R. L.; Morokuma, K.; Zakrzewski, V. G.; Voth, G. A.; Salvador, P.; Dannenberg, J. J.; Dapprich, S.; Daniels, A. D.; Farkas, Ö.; Foresman, J. B.; Ortiz, J. V.; Cioslowski, J.; Fox, D. J. Gaussian 09, revision E.01. Gaussian, Inc.: Wallingford, CT, 2009.
- (85) Weigend, F.; Ahlrichs, R. Balanced Basis Sets of Split Valence, Triple Zeta Valence and Quadruple Zeta Valence Quality for H to Rn: Design and Assessment of Accuracy. *Phys. Chem. Chem. Phys.* **2005**, *7*, 3297–3305.
- (86) Grimme, S.; Antony, J.; Ehrlich, S.; Krieg, H. A Consistent and Accurate Ab Initio Parametrization of Density Functional Dispersion

Correction (DFT-D) for the 94 elements H-Pu. J. Chem. Phys. 2010, 132, 154104.